Photodetection of DNA mismatches by dissymmetric Ru(ii) acridine based complexes

Martin Gillard, Baptiste Laramée-Milette, Quentin Deraedt, Garry S Hanan, Frédérique Loiseau, Jérôme Dejeu, Eric Defrancq, Benjamin Elias, Lionel Marcélis

Journal Name

ARTICLE

Photodetection of DNA Mismatches by Dissymmetric Ru(II) Acridine Based Complexes

Received 00th January 20xx,
Accepted 00th January 20xx

DOI: 10.1039/x0xx00000x

www.rsc.org/

Martin Gillard,[a] Baptiste Laramée-Milette,[b] Quentin Deraedt,[a] Garry S. Hanan,[b] Frédérique Loiseau,[c] Jérôme Dejeu,[c] Eric Defrancq*[c], Benjamin Elias*[a] and Lionel Marcélis*[a]

The early detection of DNA mutations such as DNA mismatches is of major interest. Indeed, accumulation of mismatches into the genome arises from deficiencies of the cellular mismatch repair machinery that is associated with several types of cancers being often resistant to classic chemotherapeutics. In this context, ruthenium(II) compounds bearing a planar extended ligand appear to be excellent candidates as DNA photoprobes since they exhibit high affinity for DNA as well as tuneable luminescence properties. Herein, we report on the synthesis of a novel dissymmetric acridine based Ru(II) complex, $[Ru(bpy)_2napp]^{2+}$, along with the study of its capability to photodetect DNA mismatches. We also investigated the origin of the mismatch photodetection capability of the complex *via* CD-melting assays and bio-layer interferometry. Interestingly, this behaviour may be attributed to a better protection of the complex excited state from non-radiative deexcitation sources (e.g., collisions with the solvent, oxygen photosensitization,…) when intercalated into well- compared to mismatched DNA.

Introduction

Cancer is a major health concern as it accounts for 18.1 million new cases and 9.6 million deaths worldwide in 2018.[1] Even if considerable progress has been made during the last decades, the current cancer treatments and diagnosis show limitations such as a poor differentiation between cancer and healthy cells, leading to undesired side effects.[2] This has stimulated the design of drugs able to specifically target a biological signature of cancer.[3, 4] In this context, the early detection of mismatch repair (MMR) deficient cancers is of high interest as these cancer cells exhibit a well differentiated genetic material due to the accumulation of DNA mismatches.[5, 6] Being of high prevalence in many cancer types cast under the generic name of Lynch syndrome,[7-9] the development of new drugs to diagnose and to treat these cancers is of major issue as they often exhibit resistance to conventional treatments.[9, 10]

Among the chemical space, metallotherapeutics and more precisely ruthenium(II) compounds appear to be attractive candidates for theranostic applications with some complexes attaining advanced stages of clinical trials.[11-18] In particular, Ru(II) complexes bearing a planar extended ligand showed a strong affinity for DNA[19] and proved to be very sensitive to their microenvironment once intercalated into the double helix. The reference of the field is the $[Ru(bpy)_2dppz]^{2+}$ (bpy = 2,2'-bipyridine; dppz = dipyrido [3,2-a:2',3'-c]phenazine) complex that has been widely studied as a DNA "light switch". Indeed, in aqueous conditions, the luminescence of the complex is totally quenched, but is recovered in the presence of DNA.[20] This behaviour was explained by a better protection of the complex from non-radiative deexcitation sources (mainly the solvent and oxygen) once intercalated into the double helix.[19-21]

Aiming to exploit the extreme sensitivity of $[Ru(bpy)_2dppz]^{2+}$ to its microenvironment for detecting DNA mismatches, some analogues have been recently designed and showed different luminescence properties in the presence of mismatches relative to totally well-matched DNA.[22-24] As a general rule, it has been shown that structural modifications of the complexes by either the use of (i) dissymmetrical planar extended ligand[24-26] or (ii) bulkier ancillary ligands[27] lead to an enhancement of the mismatch recognition capability. This has been associated with a higher binding affinity toward the mismatch sites resulting from their weaker thermodynamic stability.[28, 29]

In this context, our group has been investigating the potential of dissymmetric acridine based complexes to differentiate DNA mismatches from well-matched DNA. The Ru(II) complexes $[Ru(phen)_2dpac]^{2+}$ **1** (dpac = dipyrido[3,2-a:2',3'-c]acridine) and $[Ru(bpy)_2npp]^{2+}$ **2** (npp = naphtho[1,2-b]pyrido[3,2-f][1,7]phenanthroline) were reported to

[a] Institute of Condensed Matter and Nanosciences (IMCN), Molecular Chemistry, Materials and Catalysis (MOST), Université catholique de Louvain (UCLouvain), Place Louis Pasteur 1, bte L4.01.02, B-1348 Louvain-la-Neuve, Belgium. E-mail: benjamin.elias@uclouvain.be and lionel.marcelis@uclouvain.be
Fax: +3210474168; Tel: +3210473014
[b] Departement de Chimie, Université de Montréal, 2900 Boulevard Edouard-Montpetit, Montréal, Québec H3T 1J4, Canada.
[c] Département de Chimie Moléculaire, Université Grenoble-Alpes (UGA), UMR CNRS 5250, CS 40700, 38058 Grenoble, France. E-mail: eric.defrancq@univ-grenoble-alpes.fr

† Electronic Supplementary Information (ESI) available: See DOI: 10.1039/x0xx00000x

Please do not adjust margins

differentiate mismatches based on their luminescence properties.[26, 30] In this paper, we describe the straightforward synthesis of a new dissymmetric complex $[Ru(bpy)_2napp]^{2+}$ **3** (naphtho[2,1-b]pyrido[3,2-f][1,7]phenanthroline), along with the study of its photophysics in the absence and in the presence of well- and mismatched DNA (Fig. 1).

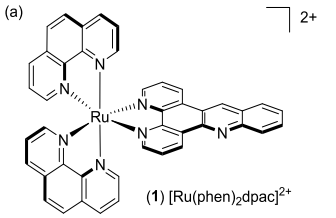

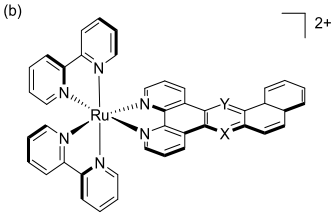

(**2**) X = CH, Y = N $[Ru(bpy)_2npp]^{2+}$
(**3**) X = N, Y = CH $[Ru(bpy)_2napp]^{2+}$

Fig. 1. Structure of complexes $[Ru(phen)_2dpac]^{2+}$ **1**, $[Ru(bpy)_2npp]^{2+}$ **2** and $[Ru(bpy)_2napp]^{2+}$ **3**.

Results

Synthetic procedures

The synthetic strategy of the **napp** ligand follows the general scheme reported by our group.[30] The key step consists in the formation of the acridine core *via* a Tröger's base modified reaction involving 5-amino-phenanthroline and amino-alcohol **7**. The preparation of amino-alcohol **7** was achieved in four steps *via* the isatin pathway starting from commercially available β-bromonaphthalene (Scheme 1). Copper (I) catalysed coupling of β-bromonaphthalene with aqueous ammonia yielded β-aminonaphthalene **4** (82% yield).[31] The isatin derivative **5** was regioselectively formed with a 78% yield by addition of di-ethyl-mesoxalate in acetic acid and subsequent air oxidation in basic conditions.[32] Next, anthranilic ester **6** was obtained in 36% yield after treatment with hydrogen peroxide in the presence of sodium methoxide followed by a decarboxylation step in acidic conditions. Lastly, reduction by $LiAlH_4$ furnished amino-alcohol **7** (90% yield). The condensation of **7** with 5-amino-phenanthroline afforded the **napp** ligand with 71% yield. The structure of **napp** was confirmed by NMR spectroscopy, HRMS spectrometry and elemental composition analysis (see the Supporting Information).

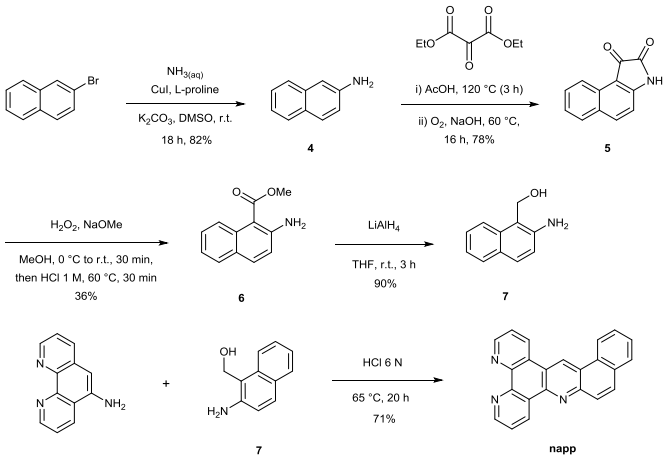

Scheme 1. Synthesis of the **napp** ligand.

$[Ru(bpy)_2napp]^{2+}$ complex **3** was synthesized by the direct chelation of **napp** ligand onto a $[Ru(bpy)_2Cl_2]$ precursor. Complex **3** was isolated as an orange solid and characterized by ^{1}H-NMR spectroscopy, HRMS spectrometry (see the Supporting Information) and X-ray crystallography (Fig. 2). ^{1}H-NMR spectroscopy shows unambiguously the absence of symmetry, which induces the non-equivalence of (i) the protons of **napp** and (ii) of the bipyridine moieties. X-ray diffraction analysis was fully consistent with NMR spectroscopy data and confirmed the structure of complex **3** in which the ruthenium(II) ion resides within an octahedral geometry. It also showed the enhanced stabilization of the packing induced by parallel displaced π-π stacking interactions between two complexes.

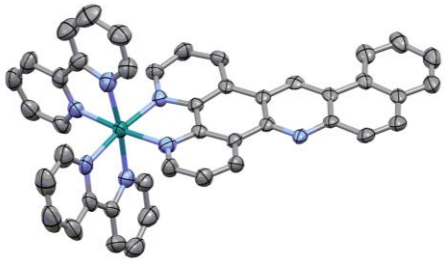

Fig. 2. X-ray crystal structure of **3**. Displacement ellipsoids of non-hydrogen atoms are drawn at the 50 % probability level. Hydrogen atoms were omitted for clarity.

Electrochemistry

The electrochemical data were obtained by cyclic voltammetry in dry deoxygenated MeCN or *N,N*-dimethylformamide (Table 1 and Supporting Information). Not surprisingly, the oxidation potential of **3** is close to that of the Ru^{2+}/Ru^{3+} oxidation of $[Ru(bpy)_3]^{2+}$ (1.34 V vs Ag/AgCl) as already observed for complexes **1** and **2**.[26] Three reversible reduction waves were detected within the investigated potential window with the less energetic reduction occurring at *ca.* -1.24 V vs Ag/AgCl, which is ascribed to the addition of an electron onto the planar extended ligand. This hypothesis is supported by the fact that phenazine containing complexes, e.g. $[Ru(bpy)_2dppz]^{2+}$ (termed **Ru-DPPZ**), display an anodically shifted reduction (≈ -1.0 V vs Ag/AgCl) than acridine ones probably due to the presence of the additional nitrogen atom which further stabilizes the added electron. Altogether, electrochemical data demonstrated that HOMO of complexes **1-3** is likely localized on the metal centre while the LUMO is localized on the planar extended ligand.

Table 1. Potentials of oxidation ($E_{1/2\ ox}$) and reduction ($E_{1/2\ red}$) of **1-3** and other reference complexes.

Complex	$E_{1/2\ ox}$ [a] [V vs Ag/AgCl]	$E_{1/2\ red}$ [b] [V vs Ag/AgCl]		
$[Ru(bpy)_3]^{2+}$	1.34	-1.28	-1.47	-1.71
$[Ru(bpy)_2dppz]^{2+}$	1.29	-0.97	-1.39	-1.62
$[Ru(phen)_2dpac]^{2+}$ **1**	1.35	-1.22	-1.35	-1.66
$[Ru(bpy)_2npp]^{2+}$ **2**	1.39	-1.23	-1.38	-1.60
$[Ru(bpy)_2napp]^{2+}$ **3**	1.35	-1.24	-1.38	-1.65

[a] Measured in dry acetonitrile. [b] Measured in dry N,N-dimethylformamide. The electrochemical data for complexes $[Ru(bpy)_3]^{2+}$, $[Ru(bpy)_2dppz]^{2+}$, $[Ru(phen)_2dpac]^{2+}$ and $[Ru(bpy)_2npp]^{2+}$ are from references.[21, 26, 30]

Light absorption data

Light absorption data were recorded at ambient temperature in water and acetonitrile under air (Table 2). The absorption spectra show typical shapes for Ru(II) complexes bearing polypyridyl ligands as described for $[Ru(bpy)_3]^{2+}$ (Fig. 3).[21] Indeed, comparison of the data obtained for **1-3** with literature allows us to assign the strong absorption bands ($\varepsilon \approx 10^5\ M^{-1}cm^{-1}$) in the UV region to ligand-centred (LC) transitions and the broad absorption bands at *ca.* 450 nm ($\varepsilon \approx 10^4\ M^{-1}cm^{-1}$) to metal-to-ligand charge-transfer (MLCT). In the case of **Ru-DPPZ**, absorption of a photon leads to the formation of a charge-separated state in which an electron is transferred from ruthenium (II) towards the phen or phenazine part of the dppz ligand.[33] In the case of complex **3**, a small bathochromic shift (Δλ = 8 nm) of the MLCT transition at 456 nm compared to **1** is noticeable as already reported for **2**. This is ascribed to the increased conjugation provided by the additional phenyl of the "elbow-shaped" ligands.

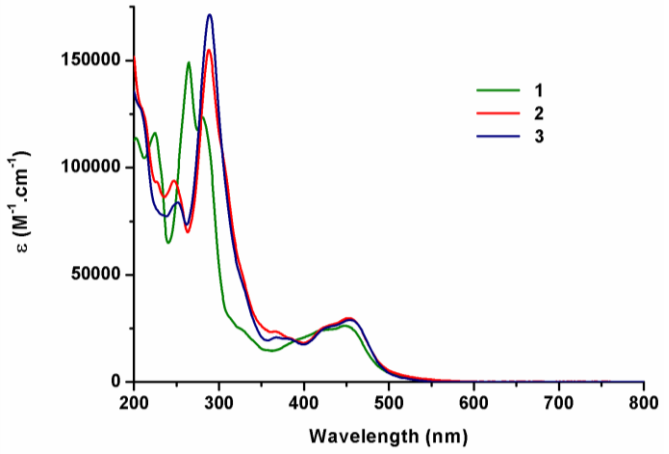

Fig. 3. Absorption spectra of complexes **1-3** in acetonitrile under air.

Table 2. Absorption data in CH_3CN and H_2O under ambient air for **1-3** and other reference complexes

Complex	Absorbance λ_{max} [nm] (ε [$10^4\ M^{-1}cm^{-1}$])[a]	
	CH_3CN	H_2O
$[Ru(bpy)_3]^{2+}$	250 (2.51), 285 (8.71), 323 (sh), 345 (sh), 452 (1.45)	250, 286, 322, 345, 451
$[Ru(bpy)_2dppz]^{2+}$	255 (4.18), 284 (9.36), 352 (sh), 357 (1.56), 366 (1.55), 448 (1.57)	255, 283, 352, 357, 365, 448
$[Ru(phen)_2dpac]^{2+}$ **1**	224 (15.1), 264 (16.3), 280, (11.6), 448 (2.62)	224, 264 (16.2), 280, 448 (2.62)
$[Ru(bpy)_2npp]^{2+}$ **2**	210 (11.1), 248 (9.21) 287 (15.6), 457 (2.94)	210, 248, 287 (15.6), 457 (2.93)
$[Ru(bpy)_2napp]^{2+}$ **3**	246 (3.31), 289 (6.82), 456 (1.24)	210, 243, 286 (6.83), 456 (1.24)

[a] Measurements were performed with 1.10^{-5} mol.L^{-1} solutions in complex at room temperature. Extinction coefficients are reported in brackets. Absorption bands in the visible region ($\varepsilon \approx 10^4\ M^{-1}\ cm^{-1}$ around $\lambda \approx 400–450$ nm) are attributed to Metal-to-Ligand Charge-Transfer (MLCT) transitions. The absorption data for complexes $[Ru(bpy)_3]^{2+}$, $[Ru(bpy)_2dppz]^{2+}$, $[Ru(phen)_2dpac]^{2+}$ and $[Ru(bpy)_2npp]^{2+}$ are from references.[21, 26, 30]

Journal Name

ARTICLE

Computational studies

To better understand the photophysics of complex **3** along with the influence of the formation of hydrogen bond with the non-chelating nitrogen of **napp** at the excited state, the ground- and excited-state electronic structures of the complex and of its protonated form in water were investigated by means of DFT/time-dependent (TD-DFT) calculations. In accordance with electrochemical data, the calculations of the electronic structures of complex **3** and of its protonated form in water locate the HOMO on the metal centre (see the Supporting Information). Concerning the LUMO of **3** in water, the calculations show a distribution between the planar extended ligands (66 % contribution) and the ancillary ligands (34 % contribution). Conversely, the LUMO of the protonated form of complex **3** appears to be fully localized on the protonated **napp** ligand. The experimental absorption spectra match well with the calculated transitions, which allows us to attribute the different transitions by using natural transitions orbitals (NTOs).[34] The less energetic transitions that occur between the HOMO and the LUMO of the complex seem to be ^{1}MLCT-type transitions that stand between the metal centred HOMO and the **napp**- (major) and bpy-centred (minor) LUMO, LUMO+1 and LUMO+3. Concerning the protonated complex, the less energetic transition appears to be a HOMO-LUMO transition occurring between the metal-centred HOMO and the fully **napp** centred LUMO. Regarding the calculations obtained for **3** and its protonated form in water, it is likely that the formation of hydrogen bond with the non-chelating nitrogen of **napp** has a strong influence on the photophysics of the complex. Indeed, the excited electron is mainly located on the planar extended ligand, which can be protonated. Therefore, in polar protic solvents such as water, the microenvironment of the **napp** ligand should play a major role on the photophysics of the complex (*vide infra*).

Light emission data

Emission, quantum yield and lifetime measurement of **3** recorded in water and in acetonitrile suggest similar photophysical properties compared to **1** and **2** (Table 3). Indeed, the three complexes exhibit typical characteristics of ^{3}MLCT-type transitions as they possess (i) a broad unstructured emission subject to strong solvatochromic effect and (ii) a relatively long (≈ microsecond) lifetime of the excited state. This ^{3}MLCT-type transition is promoted by the substantial spin orbit coupling of Ru(II). In addition, the charge-separated state character is confirmed by (i) less energetic emissions in water than in acetonitrile resulting from a better stabilization of the dipolar excited state in a more polar solvent (ii) the hypsochromic shift of the emission band at 77 K (λ_{max} = 567-577 nm) and (iii) the large k_r value (> 10^4 s^{-1}) (Table 3). A decrease in the luminescence intensity in air-equilibrated solvents compared to nitrogen-purged solutions is observed for all the complexes that indicates a photosensitization of $^3O_2$ by the excited complexes (data not shown).

Table 3. Emission data in CH_3CN and H_2O at 298 K and 77 K under ambient air for complexes **1-3** other reference complexes

	Emission λ_{max} [a,b] [nm]		Emission λ_{max} [b] at 77 K [nm]	Φ_{em} [c,d]		τ_{em} [ns] [c]		k_r [10^3 s^{-1}]	
Complex	CH_3CN	H_2O	EtOH/MeOH 4/1	CH_3CN	H_2O	CH_3CN	H_2O	CH_3CN	H_2O
$[Ru(bpy)_3]^{2+}$	604	604	578	0.062	0.042	855	630	77	69
$[Ru(phen)_3]^{2+}$	604	606	564	0.028	0.072	460	920	61	75
$[Ru(bpy)_2dppz]^{2+}$	610	—[e]	581	0.031	—[e]	692	—[e]	45	—[e]
$[Ru(phen)_2dpac]^{2+}$ **1**	597	604	567	0.038	0.066	710	999	54	66
$[Ru(bpy)_2npp]^{2+}$ **2**	604	606	577	0.083	0.092	702	750	118	123
$[Ru(bpy)_2napp]^{2+}$ **3**	601	606	576	0.072	0.12	812	841	89	143

[a] Measurements were made with solutions 1 × 10^{-5} mol.L^{-1} in complex under air. [b] λ_{exc} = 450 nm. [c] Measurements were made with solutions 1 × 10^{-5} mol L^{-1} in complex under argon. [d] Measurements relative to $[Ru(bpy)3]^{2+}$ in nitrogen purged aqueous solution (Φ_{em} = 0.063) and in nitrogen purged acetonitrile (Φ_{em} = 0.094).[35] [e] No luminescence was observed in H_2O. The photophysical data for complexes $[Ru(bpy)_3]^{2+}$, $[Ru(phen)_3]^{2+}$,[20] $[Ru(bpy)_2dppz]^{2+}$,[23] $[Ru(phen)_2dpac]^{2+}$ and $[Ru(bpy)_2npp]^{2+}$ are from references.[36-38]

The chemical modification of the acridine core *via* the addition of an aromatic ring results in a bathochromic shift of the emission maxima both in CH_3CN and H_2O. This means that the presence of the additional phenyl ring in complexes **2** and **3** leads to a better stabilization of the excited state compared to complex **1**. Interestingly, we also observed a longer excited state lifetime and increased k_r values of our complexes in water than in acetonitrile., It was also noticed that the luminescence lifetimes of complexes **1-3** are inversely related to the hydrophobic and steric hindrance around their acridine core nitrogen (**2 < 3 < 1**).

Photophysics in the presence of DNA

As shown on Fig. 4, the luminescence of complex **3** was significantly enhanced in the presence of increasing concentrations of DNA in agreement with the previously studies with complexes **1** and **2**. [26, 30]

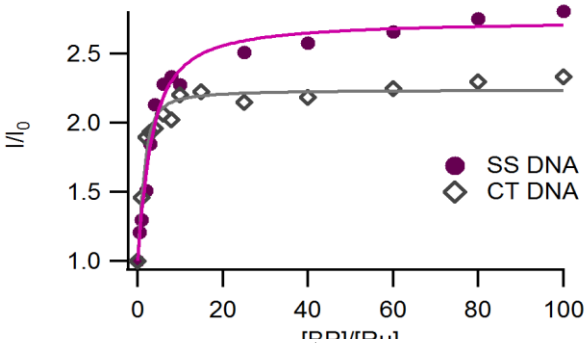

Fig. 4. Relative luminescence intensity (I/I_0) of **3** as a function of the relative DNA base pairs concentration ([BP]/[Ru]) with I_0, the luminescence of the complex in the absence of DNA (SS-DNA salmon sperm DNA full circles and Calf Thymus-DNA (empty diamonds). Measurements were performed by using 10 µM of complex in 50 mM Tris·HCl buffer, with 50 mM NaCl at pH 7.4 under ambient air conditions. Irradiation at 450 nm. The fitted curves were obtained by using a modified McGhee–von Hippel equation and drawn in purple for SS-DNA and in grey for CT-DNA.

The affinity constants of complexes **1-3** for DNA have been estimated using a modified McGhee-von Hippel model that fits the titration curves (Table 4).[39] Complex **3** exhibits a micromolar range affinity for DNA which is in agreement with our previous studies on complex **1** and **2**. Since our complexes are structurally close to **Ru-DPPZ** and possess high affinities for DNA, we assume that they also intercalate into DNA.

Table 4. Binding affinity constants estimated for **1-3** with SS-DNA and CT-DNA

	SS-DNA		CT-DNA	
Complex	K_D (µM)[a]	I/I_0 max	K_D (µM)[a]	I/I_0 max
$[Ru(phen)_2dpac]^{2+}$ **1**	0.55	2.6	2.4	2.8
$[Ru(bpy)_2npp]^{2+}$ **2**	1.3	2.7	12	2.4
$[Ru(bpy)_2napp]^{2+}$ **3**	1.2	2.7	10	2.2

[a] Binding constants were obtained by using a McGhee-von Hippel type equation; the binding site was fixed to two base pairs per complex (best fit). Errors estimated to 5%.

Photophysics in the presence of mismatched DNA

The capability of complex **3** to recognize mismatched DNA base pairs from well-matched DNA was investigated by using a series of short hairpin-shape DNA models. These hairpin DNA models contain (or not) a single mismatch base pair near the centre of the duplex (see the sequences in Fig. 5).

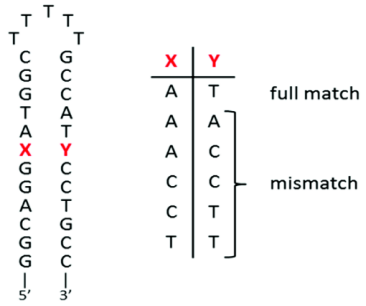

Fig. 5. Schematic representation of the short DNA hairpins used for titrations.

A 2-fold decrease of luminescence intensity has been shown for complex **1** in the presence of mismatched DNA *versus* the well-matched sequence. Nevertheless, complex **1** is unable to differentiate the different types of mismatched hairpins.[30] As mentioned previously, the elbow-shaped structure of **2** and **3** would be of interest to obtain such specificity for mismatches. Indeed, complex **2**, bearing the elbow on the non-chelating nitrogen side proved to better discriminate the different mismatches.[26]

Interestingly, complex **3,** which bears the elbow at the opposite side of the non-chelating nitrogen, showed better differentiation capabilities. Indeed, complex **3** displayed higher luminescence intensity decreases from well-matched DNA to mismatched DNA to reach a 3-fold luminescence intensity diminution for TT mismatched hairpin (Fig. 6). Furthermore, complex **3** was found able to discriminate the different mismatches with a 2-fold luminescence intensity difference between AC and TT mismatched sequences (see Fig. S22 in the Supporting Information).

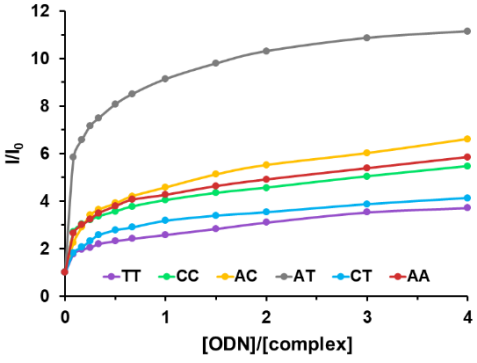

Fig. 6. Relative luminescence intensity (I/I_0) of **3** as a function of the relative hairpin oligonucleotide concentration ([ODN]/[Ru]) with I_0, the luminescence of the complex in the absence of DNA (λ_{exc} = 450 nm). Measurements were performed using 1 µM of complex in Tris·HCl buffer 5 mM, NaCl 1 mM, pH 7.5 under ambient air condition. Lines are used as eye-guides and do not correspond to a fitting process.

To better understand the origin of the difference of luminescence intensity of complex **3** between well-matched and mismatched DNA, binding affinity studies were performed by using circular dichroism (CD) melting assays and bio-layer interferometry (BLI).

Binding affinity studies

CD melting assays were implemented to assess a potential difference of affinity of complex **3** for well-matched *versus* TT-mismatched DNA sequences. The latter was chosen because it showed the largest difference in luminescence intensity with AT well-matched sequence. The measurements were carried out in the same conditions than steady state luminescence titrations (Tris·HCl buffer 5 mM, NaCl 1 mM, pH 7.5). The correct folding of well-matched and TT-mismatched oligonucleotides into double helix structure was confirmed by the presence of a negative peak at 248 nm and a positive peak at 278 nm (see Fig. S23 in the Supporting Information).[40] Upon addition of complex **3** no change in the CD spectrum was observed suggesting that the complex did not induce structural changes in the double helix structure of the hairpins. After addition of one equivalent to either well-matched or TT-mismatched hairpin, we observed an increase of the melting temperatures by 5.0 °C and 4.6 °C respectively, which indicates a stabilization of the double helix as a result of intercalation of the complex into the duplex (Table 5 and Fig. S24). However, it does not suggest a significant difference of affinity of complex **3** for any of the two hairpins.

Table 5. Melting temperatures for well-matched and TT-mismatched hairpins in the absence or presence of complex **3**.

XY	T_m (°C) (±0.5)		ΔT_m (°C) (±1)
AT	62.4[a]	67.4[b]	5.0
TT	54.3[a]	58.9[b]	4.6

Melting temperatures were measured using 2.5 µM of complex and of hairpin in Tris·HCl buffer 5 mM, NaCl 1 mM, pH 7.5 under ambient air condition. [a] Measurements performed for the hairpins alone. [b] Measurements performed in the presence of one equivalent of complex **3**.

To further determine the affinities of complex **3** for the different hairpins, we next performed bio-layer interferometry analysis. This technique allows the determination of the association and dissociation kinetic constants between the compound of interest and its target, which directly gives access to the affinity constant (such as surface plasmon resonance). BLI has been used to study biomolecular interactions between large biomolecules, such as protein–membrane interactions and more recently for the interactions of small molecules with G-quadruplex DNA.[17, 41] The six different hairpins sequences were tested in the same conditions to that of steady state luminescence titrations and CD melting assays (Tris·HCl buffer 5 mM, NaCl 1 mM, pH 7.5). As an example, BLI sensorgrams recorded for the interaction of complex **3** with the fully well-matched hairpin and the TT-mismatch containing hairpin are displayed in Fig. 7. Complex **3** exhibited affinity constants close to the micromolar for each hairpin (0.90 to 3.0 µM). Thus no noticeable difference of affinity for a particular hairpin could be revealed (Table 6).

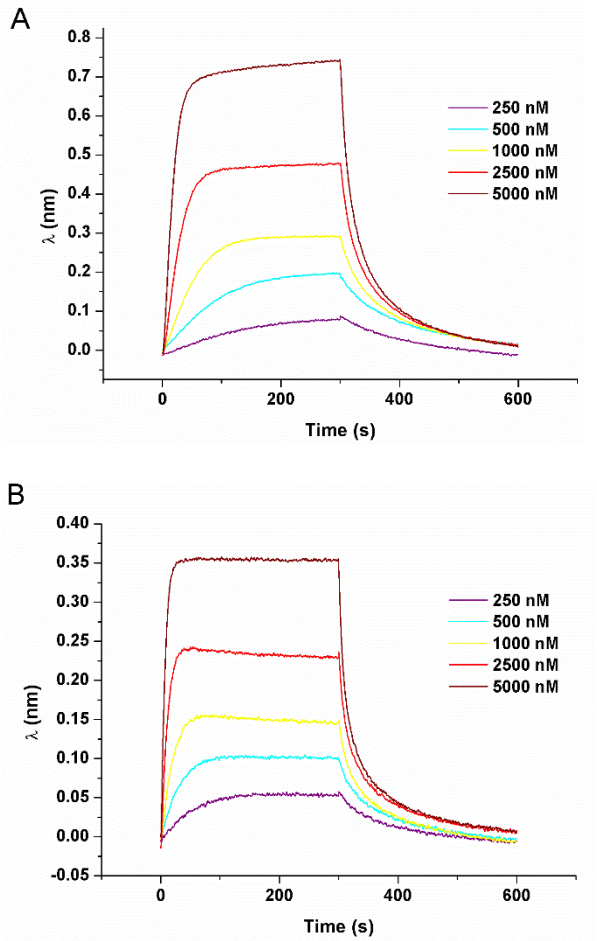

Fig. 7 BLI response curves for the association and dissociation of **3** in the presence of well-matched hairpin (A) and the TT-mismatch containing hairpin (B). Measurements are performed using 250 to 5000 nM of complex in Tris·HCl buffer 5 mM, NaCl 1 mM, pH 7.5 under ambient air condition.

Table 6. Dissociation constants estimated for **3** for the different hairpins.

XY	k_{on} (10^4 M^{-1} s^{-1})	k_{off} (10^{-2} s^{-1})	K_D (µM)
AT	0.846	2.45	2.90
AA	1.52	1.92	1.26
AC	0.933	2.78	2.98
CC	2.70	5.50	2.04
CT	3.77	3.39	0.90
TT	2.58	2.85	1.11

Equilibrium dissociation constants were deduced from the kinetic rate constants. Measurements were performed using a concentration range from 0.5 µM to 20 µM of complex in Tris·HCl buffer 5 mM, NaCl 1 mM, pH 7.5 under ambient air condition. Errors are estimated to 10%. See Fig. S25 for all the sensorgrams.

Discussion

Computational studies, electrochemical and photophysical data for complexes **1-3** allow us to study their photophysics to better understand the photophysical behaviour of the complexes alone and in the presence of DNA.

Photophysical scheme for complexes 1-3 alone

By comparing the photophysical data of acridine-based complexes **1-3** with **Ru-DPPZ**, we suggest that these systems follow a different photophysical scheme than phenazine based complexes. Indeed, it is well accepted that **Ru-DPPZ** and its derivatives are less luminescent in water than in acetonitrile since the formation of two hydrogen bonds between water and the two phenazine core nitrogen's leads to the formation of a non-emissive ^{3}MLCT "dark state".[20] In the case of acridine-based complexes, we observe the opposite trend as complexes **1-3** display longer luminescence lifetimes, increased k_r values and less energetic emission wavelengths in water with respect to acetonitrile (Table 3). As already reported for the $[Ru(phen)_3]^{2+}$ complex,[42] we assume that acridine-based complexes display a lower luminescent excited state in a more polar solvent (*e.g.* water *vs* acetonitrile), which renders the non-emissive thermally populated ^{3}MC excited state more difficult to reach. Higher stabilisation of the luminescent excited state in H_2O may also be promoted by H-bonding with the nitrogen of the acridine core.

When comparing the photophysical data of complexes **1-3**, we notice that luminescence lifetimes in H_2O appear to be correlated to the relative steric and hydrophobic hindrance around the acridine core nitrogen (**2** < **3** < **1**), which is not the case in the non-protic CH_3CN. Indeed, the more the non-chelating nitrogen is hindered, the less they can form H-bonds and the shorter is the luminescence lifetime of the complex in water (Table 3).

Based on these observations, the computational studies, the electrochemical and photophysical data, we propose a new photophysical scheme that is based on the schemes established for **Ru-DPPZ** and $[Ru(phen)_3]^{2+}$ (Scheme 2).[37, 42] As for **Ru-DPPZ**, light absorption followed by inter-system crossing (ISC) populates a ^{3}MLCT excited state centred on the bpy/phen moiety surrounding the metal centre (state A). This state then quickly converts to another more stable ^{3}MLCT in which the electron is localized solely on the acridine part of the planar extended ligand (state B). Depending on the solvent and on the acridine nitrogen accessibility, a lower mono-hydrogen bonded ^{3}MLCT (state C) can be reached, which is in thermal equilibrium with state B. Finally, a non-emissive metal centred ^{3}MC excited state may also be populated either from state B or C.

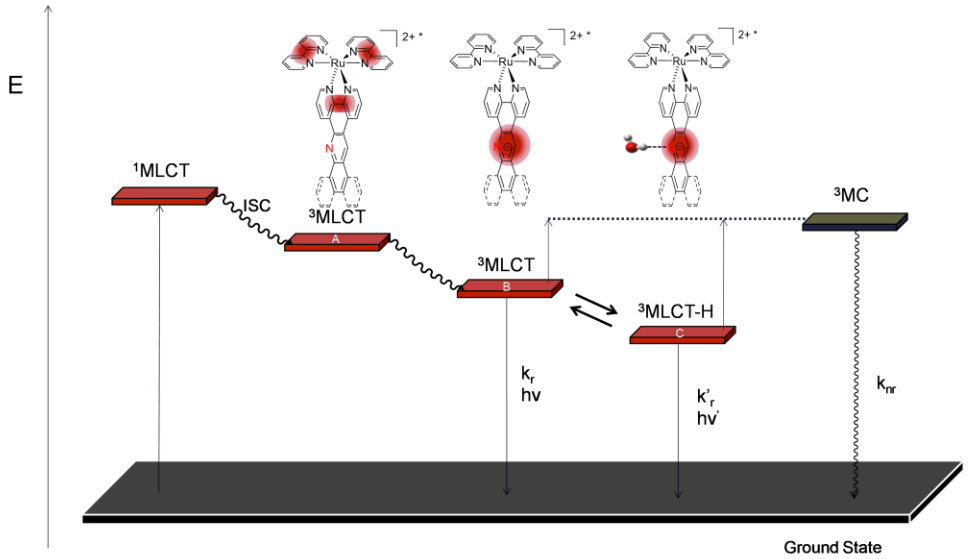

Scheme 2. Simplified photophysical scheme for Ru(II) polypyridyl metal complexes bearing an acridine based planar extended ligand.

Photophysical behaviour in the presence of DNA and mismatch containing DNA

As depicted above, the luminescence of complexes **1-3** is strongly influenced by the presence of DNA and is differently altered in the presence of mismatch containing DNA. Indeed, as already reported for other Ru(II) photoprobes, a strong enhancement of the luminescence of complex **3** in the presence of DNA was observed. This can be attributed to a protection of the complexes induced by the intercalation into DNA that prevent the excited state from non-radiative deactivation such as collisions with the solvent and oxygen photosensitization.

Besides, the fact that complexes **1-3** exhibit a significant difference of luminescence intensity between well-matched and mismatched DNA may either be explained by a difference of affinity of the complexes for mismatched DNA and/or it may arise from the high sensitivity of the complexes to their microenvironment once intercalated into DNA. According to CD melting assays and BLI, it appears that complex **3** exhibit very similar affinities for mismatch containing and totally well-matched hairpins. This means that the ability of complex **3** to photoprobe DNA mismatches does not arise from a difference in binding affinity. As a result, we assume that the origin of the intensified luminescence in the presence of well-matched compared to mismatched DNA is probably due to a better protection of the complex from non-radiative deexcitation sources when intercalated in well-matched DNA. This assumption can be supported by the fact that mismatch containing DNA is known to be less rigid which may provide better access of the solvent and oxygen to the intercalated complex leading to a lower luminescence intensity.

In addition, the fact that complex **3** displays better differentiation capabilities than **1** and **2** indicates (i) the importance of dissymmetry in the mismatch recognition process and (ii) the major role played by the non-chelating nitrogen of the acridine core in the photophysics of our complexes in the presence of DNA.

Conclusions

In this work, we report on the synthesis of a new dissymmetric acridine based ligand, **napp**, which depicts an interesting dissymmetric shape. The corresponding Ru(II) complex **3** has been fully characterized by ^{1}H-NMR and HRMS and its elbow orientation has been established by X-ray crystallography. The photophysics of **3** has been studied by computational, electrochemical and photophysical means. They suggest that the less energetic electronic transition consists in an MLCT mainly occurring between the metal core and the **napp** ligand. In addition, our results indicate that a ^{3}MLCT localized on the acridine part of the **napp** ligand in equilibrium with the hydrogen-bonded form of the complex ^{3}MLCT-H are the two main emissive states. Comparing the photophysical data obtained for **3** with the ones reported for **1** and **2** in acetonitrile and in water allowed us to propose a new photophysical scheme for acridine based Ru(II) complexes. It mainly differs from the most recent scheme described for phenazine based Ru(II) complexes as we propose that the mono-H-bonded complex is more emissive than the non-H-bonded complex due to the higher energy needed to reach the non-emissive ^{3}MC state.

Mainly, complex **3** shows interesting mismatched DNA recognition capabilities as the complex appears to be up to three times more luminescent in the presence of the fully well-matched compared to the TT-mismatch containing hairpin. The origin of this difference was investigated by using CD melting assays and bio-layer interferometry analysis. They revealed that the complex exhibits a micromolar affinity for DNA and does not possess a significant difference of affinity for the well-matched hairpin relative to the mismatch containing hairpins. The origin of the luminescence intensity difference may thus be attributed to a better protection of the complex excited state from non-radiative deexcitation sources (e.g., collisions with the solvent, oxygen photosensitization) when intercalated into well-matched DNA compared to mismatched DNA. In addition, the enhancement of the mismatch DNA recognition capability of **3** compared to **1** and **2** suggests that both the “elbow-shape” of the ligand and the hydrophobic hindrance of the non-chelating nitrogen incorporated in the planar extended ligand play an important role in the mismatch photodetection process.

Experimental

Materials and instrumentation

$[Ru(bpy)_2Cl_2]$ and 5-amino-1,10-phenanthroline were synthesized according to previously described literature protocols.[28, 43] All solvents and reagents for the synthesis were of reagent grade and were used without any further purification. All solvents for the spectroscopic and electrochemical measurements were of spectroscopic grade. Water was purified with a Millipore Milli-Q system.

Calf thymus DNA Type I (CT-DNA) and salmon sperm DNA (SS-DNA) were purchased from Sigma-Aldrich. Hairpin ODNs were purchased from Eurogentech. DNA and ODN concentrations were determined spectroscopically ($\lambda_{260\ nm}$ = 6600 M^{-1} cm^{-1} /bp for CT-DNA and SS-DNA[44, 45]; $\lambda_{260\ nm}$ = 260 000 M^{-1} cm^{-1} for ODN-AT, 264 900 M^{-1} cm^{-1} for ODN-AA, 253 300 M^{-1} cm^{-1} for ODN-CC, 259 100 M^{-1} cm^{-1} for ODN-AC, 254 200 M^{-1} cm^{-1} for ODN-CT, 257 500 M^{-1} cm^{-1} for ODN-TT). The molar extinction coefficients of hairpin oligonucleotides are values calculated based on the base content of each sequence. Biotinylated hairpin ODN’s were synthesized on a Controlled Pore Glass solid support by using the phosphoramidite approach with an Applied Biosystems 3400 DNA/RNA Synthesizer (1 μmol scale).

^{1}H NMR experiments were performed in $CDCl_3$, CD_3OD or CD_3CN on a Bruker AC-300 Avance II (300 MHz) or on a Bruker AM-500 (500 MHz) at 20 °C. The chemical shifts (given in ppm) were measured vs. the residual peak of the solvent as the internal standard. High-resolution mass spectrometry (HRMS) spectra were recorded on a Q-Exactive orbitrap from

ThermoFisher using reserpine as the internal standard. Samples were ionized by electrospray ionization (ESI; capillary temperature = 320 °C, vaporizer temperature = 320 °C, sheath gas flow rate = 5 mL min^{-1}).

Cyclic voltammetry was carried out in a one-compartment cell, using a glassy carbon disk working electrode (approximate area = 0.03 cm^2), a platinum wire counter electrode, and an Ag/AgCl reference electrode. The potential of the working electrode was controlled by an Autolab PGSTAT 100 potentiostat through a PC interface. The cyclic voltammograms were recorded with a sweep rate of 300 mV s^{-1}, in dried acetonitrile (Sigma-Aldrich, HPLC grade). The concentration of the complexes was 8 × 10^{-4} mol L^{-1}, with 0.1 mol L^{-1} tetrabutylammonium perchlorate as the supporting electrolyte. Before each measurement, the samples were purged by nitrogen.

UV-vis absorption spectra were recorded on a Shimadzu UV-1700. Room temperature fluorescence spectra were recorded on a Varian Cary Eclipse instrument. The luminescence intensity at 77 K was recorded on a FluoroLog3 FL3-22 from Jobin Yvon equipped with an 18 V, 450 W xenon short arc lamp and an R928P photomultiplier, using an Oxford Instrument Optistat DN nitrogen cryostat controlled by an Oxford Intelligent Temperature Controller (ITC503S) instrument. Luminescence lifetime measurements were performed after irradiation at λ = 400 nm obtained by the second harmonic of a Titanium/Sapphire laser (picosecond Tsunami laser spectra physics 3950-M1BB+39868-03 pulse picker doubler) at a 80 kHz repetition rate. The Fluotime 200 from AMS technologies was used for the decay acquisition. It consists of a GaAs microchannel plate photomultiplier tube (Hamamatsu model R3809U-50) followed by a time-correlated single photon counting system from Picoquant (PicoHarp300). The ultimate time resolution of the system is close to 30 ps. Luminescence decays were analyzed with FLUOFIT software available from Picoquant.

CD-analyses were recorded on a Jasco J810 spectro-polarimeter using 1 cm length quartz cuvette. Prior to CD analysis, the oligonucleotides were annealed by heating the sample at 95 °C for 5 min in the buffer conditions and cooling it overnight to room temperature. Spectra were recorded at 5 °C increments from 25 °C to 90 °C over the wavelength range from 220 to 330 nm. For each temperature, the spectrum was an average of three scans with a 0.5 s response time, a 1 nm data pitch, a 4 nm bandwidth and a 200 nm min^{-1} scanning speed. For CD melting experiments, the ellipticities of the hairpins were recorded at 248 nm. Melting temperatures were obtained using a Boltzmann-type fit on Origin software. Each curve fit was only accepted with a R value>0.99.

Bio-layer interferometry experiments were performed using sensors coated with streptavidin (SA sensors) purchased from Forte Bio (PALL). Prior to use, they were immerged for 10 minutes in buffer before functionalization to dissolve the sucrose layer. Then the sensors were dipped for 15 minutes in DNA containing solutions (biotinylated hairpin oligonucleotides) at 100 nM and rinsed in buffer solution (Tris·HCl buffer 5 mM, NaCl 1 mM, pH 7.5 and 0.5% v/v surfactant P20) for 10 minutes. The functionalized sensors were next dipped in ruthenium complex containing solution at different concentrations (see the Supporting Information) for 2 minutes interspersed by a rinsing step in the buffer solution during 4 minutes. Reference sensors without DNA immobilization were used to subtract the non-specific adsorption on the SA layer. The sensorgrams were fitted using a 1:1 interaction model. The reported values are the means of representative independent experiments, and the errors provided are standard deviations from the mean. Each experiment was repeated at least two times.

Synthetic procedures and characterization

2-aminonaphthalene. According to a modified procedure of Ma et *al*,[31] 2-bromonaphthalene (2.94 g, 14.5 mmol, 1.0 eq.), CuI (552 mg, 2.90 mmol, 0.2 eq.), L-proline (667 mg, 5.80 mmol, 0.4 eq.), and K_2CO_3 (8.00 g, 58.0 mmol, 4.0 eq.) were placed under argon. 30 mL of deoxygenated DMSO were then added to the solids followed by 15 mL of aqueous ammonia (25%, 15 eq.). The solution was stirred at 70 °C until the bromide was consumed as monitored by TLC (18 h). The mixture was then cooled and partitioned between water and ethyl acetate and the aqueous phase was extracted two times with ethyl acetate. The organic phases were then combined, washed with brine, dried over Na_2SO_4 and the solvent was evaporated *in vacuo* to afford a red-brown solid. This residue was purified on silica gel chromatography (3:1 Cy/EtOAc) to give 2-aminonaphthalene as a white solid (1.66 g, 11.6 mmol, 82%). R_f 0.24 (3:1 Cy/EtOAc); ^{1}H NMR ($CDCl_3$, 300 MHz) δ 7.72-7.63 (2H, m, $H_{7\text{-}6}$), 7.60 (d, *J* = 8.2 Hz, 1H, H_4), 7.59 (d, *J* = 8.2 Hz, 1H, H_3), 7.25-7.19 (m, 1H, H_5), 6.98 (s, 1H, H_1), 6.94 (1H, dd, *J* = 8.5, 2.3 Hz, H_8), 3.81 (s, broad, 2H, NH_2). *Data are consistent with literature values*.[46]

1H-benzo[e]indole-1,2(3H)-dione. According to a modified procedure of Bruice et *al*,[47] 2-aminonaphthalene (1.60 g, 11.2 mmol, 1.0 eq.) was placed in 90 mL of glacial acetic acid in a round bottom flask fitted with condenser and calcium chloride drying tube. The solution was heated until the complete dissolution of 2-aminonaphthalene and diethylmesoxalate (2.04 g, 11.7 mmol, 1.05 eq.) was then added. The solution was stirred at 120 °C for three hours. Afterwards, the solvent was removed *in vacuo* to deliver a red-brown solid. This solid was then washed with hydrochloric acid (1 M) and suspended in 75 mL of a sodium hydroxide solution (1 M). The solution was stirred overnight at 60 °C over a slow stream of air. The orange solution obtained was acidified to pH 3 with hydrochloric acid and the red solid was filtered off after one hour of refrigeration and dried *in vacuo*. Following the procedure of Karpenko et al.,[48] the residue was finally purified by recrystallization from boiling toluene which gave 1H-benzo[e]indole-1,2(3H)-dione as a bright red solid (1.71 g, 8.66 mmol, 78%). R_f 0.24 (2:1 Cy/EtOAc); ^{1}H NMR (CD_3CN, 300 MHz) δ 8.89 (1H, s, N*H*), 8.49 (1H, dd, *J* = 8.3, 0.9 Hz, H_5), 8.17 (1H d, *J* = 8.6 Hz H_4), 7.87 (1H, d, *J* = 8.2 Hz, H_8), 7.67 (1H, ddd, *J* = 8.3, 7.0, 1.2 Hz, H_7), 7.44 (1H, ddd, *J* = 8.2, 7.0, 1.2 Hz, H_6), 7.20 (1H, d, *J* = 8.6 Hz, H_3). *Data are consistent with literature values*.[48]

Methyl 2-amino-1-naphthoate. According to a modified procedure of Reissenweber and Mangold,[32] 1H-benzo[e]indole-1,2(3H)-dione (1.10 g, 5.58 mmol, 1.0 eq.) was suspended in MeOH (0.1 M). Sodium methoxide (30%, 4.75 mL, 3.0 eq.) was then added to the solution. After slow addition of hydrogen peroxide (50%) (227 mg, 6.70 mmol, 1.2 eq.) to the mixture at 0 °C, the initial dark violet solution turned to colourless. The reaction medium was stirred at room temperature for 30 min. The mixture was then acidified by the addition of HCl (1 M, 5 eq.) and stirred at 50 °C for 30 min. The solution was extracted from water with dichloromethane and the solvent was evaporated *in vacuo*. The residue was finally purified by silica gel chromatography (6:4 CH_2Cl_2/Cy) to afford methyl 2-amino-1-naphthoate as a white solid (390 mg, 0.423 mmol, 36%). R_f 0.28 (6:4 CH_2Cl_2/Cy); ^{1}H NMR ($CDCl_3$, 300 MHz) δ 8.38 (1H, d, *J* = 8.8 Hz, H_8), 7.55 (2H, m, H_4, H_5), 7.38 (1H, ddd, *J* = 8.6, 6.9, 1.5 Hz, H_7), 7.15 (1H, ddd, *J* = 8.0, 6.9, 1.0 Hz, H_6), 6.71 (1H, d, *J* = 8.9 Hz, H_3), 5.72 (2H, s, NH_2), 3.91 (3H, s, O*Me*).

(2-aminonaphthalen-1-yl) methanol. The methyl 2-amino-1-naphthoate (350 mg, 1.74 mmol, 1.0 eq.) was dissolved in dry THF (1M). This solution was then added dropwise to a solution of $LiAlH_4$ (197 mg, 5.22 mmol, 3.0 eq.) in dry THF (0.4 M) at 40 °C. After a 3 h stirring at r.t., EtOAc (25.0 mL) was added, followed by a solution of NaOH 1M (10 mL) until the effervescence stopped. Distilled water (10 mL) was then added to end the quenching. The organic phase was separated and the aqueous phase was finally extracted with EtOAc (3x 25 mL) which gave (2-aminonaphthalen-1-yl) methanol as a dark red solid (271 mg, 1.57 mmol, 90%). ^{1}H NMR ($CDCl_3$, 300 MHz) δ 7.94 (1H, d, *J* = 8.6 Hz, H_5), 7.72 (1H d, *J* = 7.1 Hz H_8), 7.65 (1H, d, *J* = 8.7, Hz, H_4), 7.44 (1H, ddd, *J* = 8.4, 6.9, 1.4 Hz, H_6), 7.25 (1H, ddd, *J* = 7.9, 6.8, 0.9 Hz, H_7), 6.96 (1H, d, *J* = 8.7 Hz, H_3), 5.10 (2 H, s, CH_2OH).

Napp. According to a procedure of Deraedt and Elias,[30] 5-amino-1,10-phenanthroline (187 mg, 0.956 mmol, 1.0 eq.) and (2-aminonaphthalen-1-yl)methanol (164 mg, 0.959 mmol, 1.0 eq.) were suspended in 6N HCl (7 mL). The solution was stirred for 20 h at 65 °C. The mixture was then cooled down to room temperature and the acidity was quenched by addition of aqueous ammonia until pH 9. The so formed orange precipitate was filtered and washed with water. The solid was finally purified by neutral alumina chromatography (CH_2Cl_2 to 9:1 CH_2Cl_2/MeOH) to afford naphtho[2,1-b]pyrido[3,2-f][1,7]phenanthroline (**napp**) as a beige solid (224 mg, 0.679 mmol, 71%). ^{1}H NMR ($CDCl_3$, 500 MHz) δ 10.09 (1H, s, H_d), 9.61 (1H, dd, J_{a-b} = 8.1, J_{a-c} = 1.8 Hz, H_a), 9.29 (1H, dd, J_{k-l} = 8.3, J_{k-m} = 1.4 Hz, H_k), 9.14 (1H, dd, J_{c-b} = 4.3, J_{c-a} = 1.8 Hz, H_c), 9.10 (1H, dd, J_{m-l} = 4.3, J_{m-k} = 1.5 Hz H_m), 9.04 (1H, d, J_{e-f} = 8.2 Hz, H_e), 8.12 (1 H, d, J_{j-i} = 9.1 Hz, H_j), 8.05 (1 H, d, J_{j-i} = 9.2 Hz, H_j), 8.03 (1 H, d, J_{h-g} = 7.3 Hz, *H*), 7.85-7.79 (2 H, m, $H_{f,g}$), 7.79-7.74 (2 H, m, $H_{l,b}$); HRMS-ESI calculated for $C_{23}H_{14}N_3$ ($[M+H]^+$) : *m/z* 332.11822, found: *m/z* 332.11816.

$[Ru(bpy)_2napp]^{2+}$ 3. The $[Ru(bpy)_2Cl_2]$ precursor (20 mg, 0.041 mmol, 1.0 eq.) and **napp** (20 mg, 0.061 mmol, 1.5 eq) were mixed in a solution of absolute ethanol/water (5/5 - v/v, 5 mL). The reaction mixture was then stirred at 80 °C until the ligand was consumed as monitored by TLC (3 h). Afterwards, ethanol was evaporated and addition of small portions of NH_4PF_6 yielded to the formation of an orange precipitate. After centrifugation, the solid was washed several times with water and was then dried *in vacuo*. The so formed orange-red crude was finally purified on silica gel chromatography (10:1:0.5 CH_3CN/H_2O/ KNO_{3sat}) to afford $[Ru(bpy)_2napp]^{2+}$ **3** as an orange solid (28 mg, 0.027 mmol, 66%). The counter-anion exchange from PF_6^- to Cl^- was performed by adding small portions of NBu_4Cl to a solution of the complex in acetone. R_f 0.35 (CH_3CN/H_2O/ KNO_{3sat} 10:1:1/2); ^{1}H NMR (CD_3CN, 500 MHz) δ (ppm), 10.47 (1H, s, H_d), 9.81 (1H, d, J_{a-b} = 8.2, J_{a-c} = 1.2 Hz, *Ha*), 9.59 (1H, dd, J_{c-b} = 8.2, J_{c-a} = 1.2 Hz, H_c), 9.24 (1H, d, J_{m-l} = 8.2 Hz, H_m), 8.53 (4H, m, H_5, $H_{5'}$, H_6, $H_{6'}$), 8.34 (1H, d, J_{i-j} = 9.1 Hz, H_i), 8.25 (1H, d, J_{j-i} = 9.1 Hz, H_j), 8.16 (2H, m, H_4, $H_{4'}$), 8.12 (3H, m, H_e, H_f, H_g), 8.01 (2H, m, H_7, $H_{7'}$), 7.95 (1H, m, H_l), 7.91-7.84 (5H, m, H_b, H_2, $H_{2'}$, H_m, H_h), 7.73 (1H, d, J_{9-8} = 5.4 Hz, H_9), 7.69 (1H, d, $J_{9'-8'}$ = 5.6 Hz, $H_{9'}$), 7.49-7.44 (2H, m, H_3, $H_{3'}$), 7.28-7.21 (m, 2H, H_8, $H_{8'}$); HRMS-ESI calculated for $[C_{43}H_{29}N_7F_6PRu]^+$: *m/z* 890.11728, found: *m/z* 890.11700 and for $[C_{43}H_{29}N_7Ru]^{2+}$: *m/z* 372.57617, found: *m/z* 372.57640. The product yielding was confirmed by elemental composition analysis and X-ray crystallography.

Conflicts of interest

The authors declare no competing interest.

Acknowledgements

M. G. and B. E. gratefully acknowledge the Université catholique de Louvain, the Fonds National pour la Recherche Scientifique (F.R.S.-F.N.R.S.) and the Prix Pierre et Colette Bauchau for financial support. We also thank Dr. Koen Robeyns for scientific and technical support. B. L.-M. and G. S. H. thank the Natural Sciences and Engineering Research Council (NSERC) of Canada for financial support. The NanoBio-ICMG platform (FR 2607) is acknowledged for the technical support. This work was supported by IDEX Grenoble and the Region Auvergne-Rhône-Alpes for financial support. We also thank Oceane Thery and Hugues Bonnet for technical support.

References

1

1. F. Bray, J. Ferlay, I. Soerjomataram, R. L. Siegel, L. A. Torre and A. Jemal, *CA Cancer J. Clin.*, 2018, **68**, 394-424.
2. W. Marx, N. Kiss, A. L. McCarthy, D. McKavanagh and L. Isenring, *J. Acad. Nutr. Diet.*, 2016, **116**, 819-827.
3. S. A. Dugger, A. Platt and D. B. Goldstein, *Nat. Rev. Drug Discov.*, 2017, **17**, 183.
4. D. M. Hyman, B. S. Taylor and J. Baselga, *Cell*, 2017, **168**, 584-599.
5. D. Guillotin and S. A. Martin, *Exp. Cell Res.*, 2014, **329**, 110-115.

6. G. Ponti, M. Manfredini, A. Tomasi and G. Pellacani, *Gene*, 2016, **589**, 127-132.
7. C. Rosty, M. D. Walsh, N. M. Lindor, S. N. Thibodeau, E. Mundt, S. Gallinger, M. Aronson, A. Pollett, J. A. Baron, S. Pearson, M. Clendenning, R. J. Walters, B. N. Nagler, W. J. Crawford, J. P. Young, I. Winship, A. K. Win, J. L. Hopper, M. A. Jenkins and D. D. Buchanan, *Fam. Cancer*, 2014, **13**, 573-582.
8. J. M. Helder-Woolderink, E. A. Blok, H. F. A. Vasen, H. Hollema, M. J. Mourits and G. H. De Bock, *Eur. J. Cancer*, 2016, **55**, 65-73.
9. P. Boland, M. Yurgelun and R. Boland, *CA Cancer J. Clin.*, 2018, **68**, 217-231.
10. F. Honecker, H. Wermann, F. Mayer, A. J. Gillis, H. Stoop, R. J. van Gurp, K. Oechsle, E. Steyerberg, J. T. Hartmann, W. N. Dinjens, J. W. Oosterhuis, C. Bokemeyer and L. H. Looijenga, *J. Clin. Oncol.*, 2009, **27**, 2129-2136.
11. D.-L. Ma, T. Xu, D. S.-H. Chan, B. Y.-W. Man, W.-F. Fong and C.-H. Leung, *Nucleic Acids Res.*, 2011, **39**, e67-e67.
12. D. S.-H. Chan, H.-Z. He, C.-H. Leung and D.-L. Ma, *Nucleic Acids Res.*, 2013, **41**, 4345-4359.
13. C. Mari, V. Pierroz, S. Ferrari and G. Gasser, *Chem. Sci.*, 2015, **6**, 2660-2686.
14. F. E. Poynton, S. A. Bright, S. Blasco, D. C. Williams, J. M. Kelly and T. Gunnlaugsson, *Chem. Soc. Rev.*, 2017, **46**, 7706-7756.
15. S. Thota, D. A. Rodrigues, D. C. Crans and E. J. Barreiro, *J. Med. Chem.*, 2018, **61**, 5805-5821.
16. G. Piraux, L. Bar, M. Abraham, T. Lavergne, H. Jamet, J. Dejeu, L. Marcélis, E. Defrancq and B. Elias, *Chem. Eur. J.*, 2017, **23**, 11872-11880.
17. J. Weynand, A. Diman, M. Abraham, L. Marcélis, H. Jamet, A. Decottignies, J. Dejeu, E. Defrancq and B. Elias, *Chem. Eur. J.*, 2018, **24**, 19216-19227.
18. K. Lin, Z.-Z. Zhao, H.-B. Bo, X.-J. Hao and J.-Q. Wang, *Front. Pharmacol.*, 2018, **9**.
19. H.-K. Liu and P. J. Sadler, *Acc. Chem. Res.*, 2011, **44**, 349-359.
20. A. E. Friedman, J. C. Chambron, J. P. Sauvage, N. J. Turro and J. K. Barton, *J. Am. Chem. Soc.*, 1990, **112**, 4960-4962.
21. E. Amouyal, A. Homsi, J.-C. Chambron and J.-P. Sauvage, *J. Chem. Soc., Dalton Trans.*, 1990, 1841-1845.
22. A. Granzhan, N. Kotera and M.-P. Teulade-Fichou, *Chem. Soc. Rev.*, 2014, **43**, 3630-3665.
23. J. K. Barton, A. N. Boynton and K. M. Boyle, in *DNA-targeting Molecules as Therapeutic Agents*, The Royal Society of Chemistry, 2018, pp. 367-390.
24. A. N. Boynton, L. Marcélis, A. J. McConnell and J. K. Barton, *Inorg. Chem.*, 2017, **56**, 8381-8389.
25. A. J. McConnell, M. H. Lim, E. D. Olmon, H. Song, E. E. Dervan and J. K. Barton, *Inorg. Chem.*, 2012, **51**, 12511-12520.
26. Q. Deraedt, L. Marcelis, F. Loiseau and B. Elias, *Inorg. Chem. Front.*, 2017, **4**, 91-103.
27. A. N. Boynton, L. Marcélis and J. K. Barton, *J. Am. Chem. Soc.*, 2016, **138**, 5020-5023.
28. E. Rüba, J. R. Hart and J. K. Barton, *Inorg. Chem.*, 2004, **43**, 4570-4578.
29. M. H. Lim, H. Song, E. D. Olmon, E. E. Dervan and J. K. Barton, *Inorg. Chem.*, 2009, **48**, 5392-5397.
30. Q. Deraedt, L. Marcélis, T. Auvray, G. S. Hanan, F. Loiseau and B. Elias, *Eur. J. Inorg. Chem.*, 2016, **2016**, 3649-3658.
31. L. Jiang, X. Lu, H. Zhang, Y. Jiang and D. Ma, *J. Org. Chem.*, 2009, **74**, 4542-4546.
32. G. Reissenweber and D. Mangold, *Angew. Chem. Int. Ed.*, 1981, **20**, 882-883.
33. R. M. Hartshorn and J. K. Barton, *J. Am. Chem. Soc.*, 1992, **114**, 5919-5925.
34. R. L. Martin, *J. Chem. Phys.*, 2003, **118**, 4775-4777.
35. A. M. Brouwer, *Pure Appl. Chem.*, 2011, **83**, 2213-2228.
36. J. V. Caspar and T. J. Meyer, *J. Am. Chem. Soc.*, 1983, **105**, 5583-5590.
37. J. Olofsson, B. Önfelt and P. Lincoln, *J. Phys. Chem. A*, 2004, **108**, 4391-4398.
38. I. Ortmans, B. Elias, J. M. Kelly, C. Moucheron and A. Kirsch-DeMesmaeker, *Dalton Trans.*, 2004, 668-676.
39. J. D. McGhee and P. H. von Hippel, *J. Mol. Biol.*, 1974, **86**, 469-489.
40. J. Kypr, I. Kejnovská, D. Renciuk and M. Vorlícková, *Nucleic Acids Res.*, 2009, **37**, 1713-1725.
41. J. Wallner, G. Lhota, D. Jeschek, A. Mader and K. Vorauer-Uhl, *J. Pharm. Biomed. Anal.*, 2013, **72**, 150-154.
42. A. Boisdenghien, C. Moucheron and A. Kirsch-De Mesmaeker, *Inorg. Chem.*, 2005, **44**, 7678-7685.
43. S. Ji, H. Guo, X. Yuan, X. Li, H. Ding, P. Gao, C. Zhao, W. Wu, W. Wu and J. Zhao, *Org. Lett.*, 2010, **12**, 2876-2879.
44. E. M. Castanheira, M. S. D. Carvalho, A. R. O. Rodrigues, R. C. Calhelha and M.-J. R. Queiroz, *Nano. Res. Lett.*, 2011, **6**, 379.
45. R. B. Dixit, T. S. Patel, S. F. Vanparia, A. P. Kunjadiya, H. R. Keharia and B. C. Dixit, *Sci. Pharm.*, 2011, **79**, 293-308.
46. G. D. Vo and J. F. Hartwig, *J. Am. Chem. Soc.*, 2009, **131**, 11049-11061.
47. T. C. Bruice, *J. Am. Chem. Soc.*, 1957, **79**, 702-705.
48. A. S. Karpenko, M. O. Shibinskaya, N. M. Zholobak, Z. M. Olevinskaya, S. A. Lyakhov, L. A. Litvinova, M. Y. Spivak and S. A. Andronati, *Pharm. Chem. J.*, 2006, **40**, 595-602.